Real-Time Wind Measurement in Extratropical Cyclones by Means of Doppler Radar

H. W. BAYNTON, R. J. SERAFIN, C. L. FRUSH AND G. R. GRAY

National Center for Atmospheric Research,[1] Boulder, Colo. 80307

P. V. HOBBS, R. A. HOUZE, JR., AND J. D. LOCATELLI

Department of Atmospheric Sciences,[2] University of Washington, Seattle 98195

(Manuscript received 4 February 1977, in revised form 6 August 1977)

ABSTRACT

Color displays of the velocities of precipitation particles detected with a C-band Doppler radar in widespread cyclonic storms provide a variety of real-time information on the atmospheric wind field.

Vertical profiles of wind speed and direction indicated by the real-time color displays agree well with rawinsonde measurements. Veering winds (or warm advection) produce a striking S-shaped pattern on the color display and backing winds (or cold advection) produce a backward S. A maximum in the vertical profile of wind speed is indicated by a pair of concentric colored rings, one upwind and one downwind of the radar. Vertically sloping velocity maxima are indicated by asymmetries in the color displays, as are confluent and difluent winds. Divergence and convergence computed from the real-time color displays are of reasonable magnitude.

1. Introduction

A C-band Doppler radar developed by the Field Observing Facility of the National Center for Atmospheric Research (NCAR) has been used to obtain measurements in extratropical cyclonic storms in the Pacific Northwest as part of the University of Washington's CYCLES (Cyclonic Extratropical Storms) Project. The radar is equipped with a real-time Doppler processor (Lhermitte, 1972) and a color display (Gray *et al.*, 1975) for showing velocities or range-normalized reflectivities. As the antenna was rotated about a vertical axis at a series of constant elevation angles, detailed displays were obtained of the radial component of the target velocity in coordinates of slant range and azimuth. Each display was protrayed in 15 colors with a velocity resolution of 2 m s^{-1}.

Lhermitte and Atlas (1961) first described how the Velocity Azimuth Display (VAD) could be used to measure the horizontal wind field in stratiform precipitation. Later work as exemplified by Browning and Wexler (1968) extended the measurement of divergence and deformation as well. The real-time color presentation described here provides essentially a multiplicity of VAD's which may be viewed simultaneously thus permitting real-time estimates of the complete horizontal wind profile within the precipitating region.

Techniques of pattern recognition are described for detecting veering and backing winds and wind velocity maxima. Confluence and difluence are also detectable and the presence of convergence is sometimes evident from inspection of the display. Procedures for computing wind profiles and convergence are given and the results of such computations are presented. Being presented with this operationally useful information, the investigator is able to opitmize his deployment of aircraft, radars, rawinsondes, etc., in real time and concentrate the rigorous analyses, after the fact, on the more interesting situations.

2. Elements of the colored Doppler velocity patterns

Pulsed Doppler radars are characterized by a maximum unambiguous velocity (V_{max}) given by

$$V_{max} = (\mathrm{PRF})(\lambda/4), \tag{1}$$

where PRF is the pulse repetition frequency (Hz), and λ the radar wavelength. For the NCAR C-band radar, $\lambda = 0.0545$ m, and for the CYCLES Project the PRF was set at 1071 Hz. Hence $V_{max} = 14.60$ m s^{-1}.

Velocities greater than the maximum unambiguous velocity are "folded over" and then assigned values less than the maximum unambiguous velocity. In practice, with the color display, there is no difficulty in resolving these ambiguities provided that the targets are spatially continuous. Velocities ranging between $\pm|V_{max}|$ are assigned, unambiguously, one of 15 colors. In the CYCLES Project, the width of each color band was

[1] The National Center for Atmospheric Research is sponsored by the National Science Foundation.

[2] Department of Atmospheric Sciences Contribution No. 433.

thus simply 2 (14.60)/15 = 1.95 m s^{-1}. Grey is used to indicate targets with radial velcoities of 0±0.97 m s^{-1}. Ground clutter, as well as all targets viewed from a direction normal to their velocity, have zero radial velocity and therefore appear grey, no matter how fast they may be moving.

The TV monitor or color display can be thought of as a fine-mesh grid. Each square of the grid is assigned one of the 15 colors corresponding to the observed radial velocity of targets, or black if there are no targets. The 15 colors are also numbered sequentially, +7 through 0 to −7, where +7 and −7 correspond to the maximum unambiguous velocity away from and toward the radar. If the velocity toward the radar rises above 14.60 m s^{-1} (in magnitude), the display will shift from color −7 (purple) to +7 (red). If further increases occur, the colors will sequence through +6, +5, etc. The fifteenth color in this kind of sequence is grey, which would represent 29.2±0.97 m s^{-1} in magnitude, the sign being determined by the context. Clearly, if the target is a spatially continuous one, extending all the way out from the radar, there is no ambiguity. However, with isolated targets, there is ambiguity, since the same color might represent several different velocities.

Also contributing to the patterns on the TV monitor is the increase in height of the radar beam with increasing slant range. Using the $\frac{4}{3}$-earth-radius convention (Battan, 1973) to allow for average refraction and earth curvature, we have

$$z = \frac{R^2}{17\,000} + R \sin\alpha, \qquad (2)$$

where z is the height (km) of the beam above the surface at slant range R (km) and α is the elevation angle. Finally, since strong thermal gradients characterize extratropical cyclones, winds change in both direction and speed with changing height.

To illustrate how these elements are combined by the color display into a colored picture, we consider a typical winter wind profile for Seattle. Fig. 1 shows the distribution of radial components, with slant range and azimuth, for this profile. Concentric arcs on the figure are drawn at increasing slant ranges to correspond to beam heights of 1, 2, 3, 4, 5, 6 and 7 km. Radial components are then plotted along each height contour. The dashed lines show where the boundaries of the dark green color (number, −1) would lie. When Fig. 1 is expanded to the full circle and radial velocity contours are drawn at the color boundaries, Fig. 2 is obtained. Observing that winds veer with height for this profile, we note that the zero velocity band (grey on the color display) bisects the picture in the shape of an S. When winds back with height, the grey traces a backward S.

3. Pattern recognition

Qualitative information about the wind field is available in real time based on pattern recognition. Some examples are given below.

a. Patterns typical of warm advection and warm fronts

When there is warm air advection, winds veer with height and, as we have already seen from our consideration of the typical winter wind profile for Seattle, the

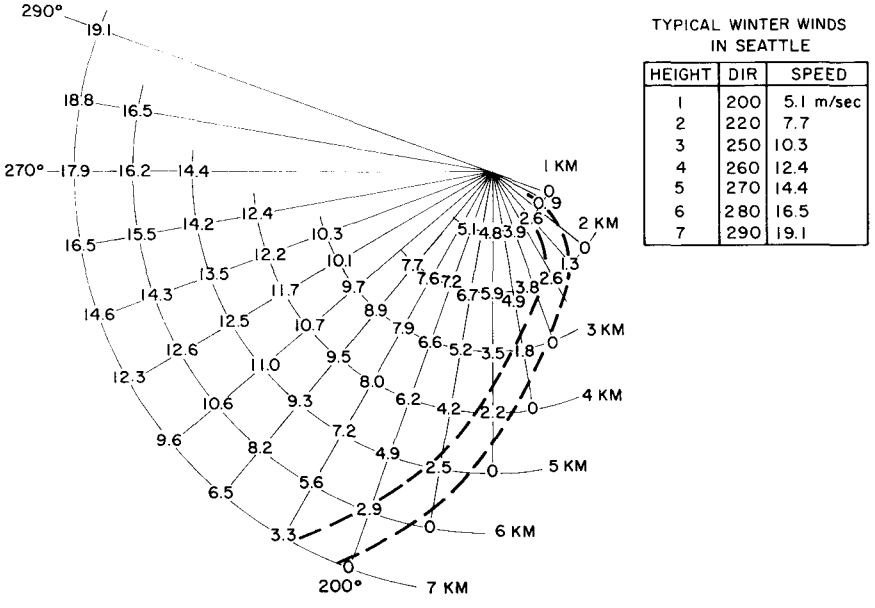

FIG. 1. Radial components of typical winter winds at Seattle. Coordinates are azimuth (deg) and slant range corresponding to beam heights of 1–7 km. Dashed lines show boundaries of the dark green region on the radar color display.

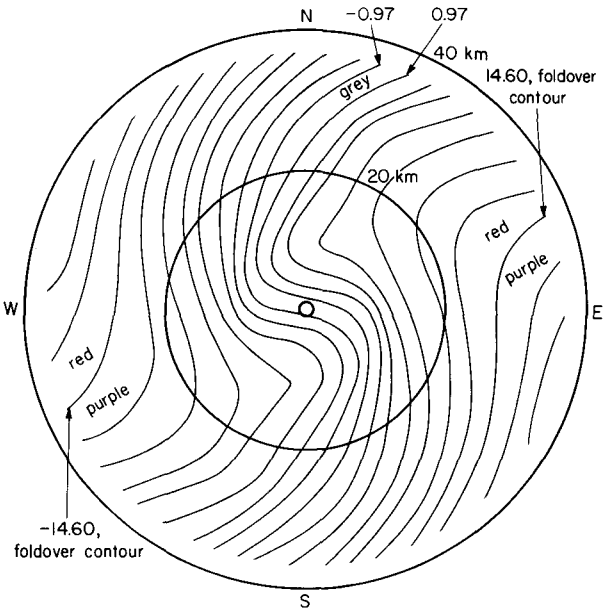

FIG. 2. Contours of radial components constructed from the typical winter wind profile for Seattle for an elevation angle of 11°. Contours are drawn at intervals of 1.95 m s^{-1} corresponding to the width of each color band in the color display.

band of zero velocities then bisects the display in the shape of an S. Color displays with this feature were common in the CYCLES Project during the winters of 1974–75 and 1975–76. Fig. 3, observed at 2205 PST 13 January 1976, is typical. Fig. 3 also illustrates a feature of the color display whereby any of the fifteen colors—here grey—can be replaced by white.

When the radar beam penetrates a warm front, an S-shaped warm advection pattern is seen on the color display in the baroclinic zone below the frontal surface, with little evidence of wind shear appearing in the relatively uniform air mass above the warm frontal surface. An example of a warm frontal pattern was observed at 2036 PST 26 January 1976 (Fig. 4). With the echo extending to a height of 5 km, virtually all of the wind shear occurred below 1.2 km, the apparent height of the warm frontal surface.

b. *Pattern typical of occlusions*

Complex thermal gradients are typically associated with occlusions (e.g., see Kreitzberg, 1964; Elliott and Hovind, 1965; Kreitzberg and Brown, 1970; Browning *et al.*, 1973; Houze *et al.*, 1976). Cold advection in the lowest layers might be accompanied by warm advection aloft or vice versa. During January 1976 mixed patterns of both types were observed. A striking example of warm advection below and cold advection aloft was observed on 22 January. Fig. 5 is the color display obtained at 0705 PST. The picture was bisected by a perfect S between the surface and 1.9 km, while above 1.9 km the pattern was reversed by backing winds. Fig. 6 is a black and white drawing based on Fig. 5 showing a wind profile derived from the colored velocity pattern. The procedure for obtaining the wind profile is explained in the caption of Fig. 6. Hodographs for the layers 0.4–1.9 km and 1.9–4.2 km, included as inserts in Fig. 6, verify the presence of warm advection in the lower layer and cold advection in the upper layer.

c. *Wind maxima*

A maximum in the vertical profile of horizontal wind speed above the radar is indicated by a pair of concentric colored rings, one upwind and one downwind, around a maximum radial velocity core. Such a wind maximum may be seen inside the innermost slant range (or height) circle in Fig. 3. The storm of 14 January 1976, producing the display shown in Fig. 7, featured two wind maxima, one at a height of about 1.8 km and another at about 4 km. Although the color display provides no information as to the lateral extent of a wind maximum, estimates can be made of the height and magnitude of the maximum wind, both upwind and downwind. Height is determined from the slant range and elevation using Eq. (2).

From upwind and downwind estimates of height, wind maxima often appear to be sloping in the vertical. On 14 January 1976 the higher altitude wind maximum has a slope of 1:30 or 1.8°. The lower wind maximum zone is nearly horizontal. Several wind maxima, with slopes from 0.6° to 1.8° have been observed in the CYCLES Project, all sloping upward in the downwind direction. These slopes must be accepted as real since the radar antenna is aligned to an accuracy of 0.1° using a plumb line, a clinometer and the sun's C-band radiation as a target with known coordinates.

It is tempting to assume that the observed wind maximum zones were due to continuous jets of air which followed a sloping path over the radar. However, such an interpretation applied to the upper wind maximum zone of Fig. 7 would imply an upward velocity of 1 m s^{-1}, a value typical of cumulus-scale convection, but not of broader mesoscale precipitation areas such as the one containing the wind maximum seen in Fig. 7. Consequently, we reject the hypothesis of a continuous upward-sloping jet and suggest instead that air at all levels moved horizontally through the upward-sloping zone of maximum wind speed.

d. *Asymmetric patterns*

If the wind field within the echo region is uniform, the measured Doppler velocity will exhibit symmetry, except for the contribution due to the vertical motion of the particles. In the cases described here, since the elevation angle was 7° and the combination of fallspeed and vertical air motion was generally less than 3 m s^{-1}, this contribution would be at most 0.4 m s^{-1} (i.e., 3 sin7°). But an asymmetry of at least 1.95 m s^{-1} is

needed to be detected as a color change. Accordingly, any observed asymmetric patterns in the display can be related to some nonuniformity of the wind field. The example of an upward sloping wind maximum has already been given. The evidence was that the slant range of the wind maximum was greater downwind than upwind. Another kind of asymmetry is evident in Fig. 4, which shows a display typical of a warm front. It is also a good example of difluence.

A quick test for difluence or confluence is to lay a straight edge across the display from the middle of the zero-velocity band on one side and through the center of the display. If the straight edge does not intercept the middle of the band at the same range on the opposite side of the radar, the flow is either difluent or confluent. Applying this test to Fig. 4, at a slant range of 40 km ($z=5$ km), shows that the wind direction is 247° north of the radar and 260° south of the radar.

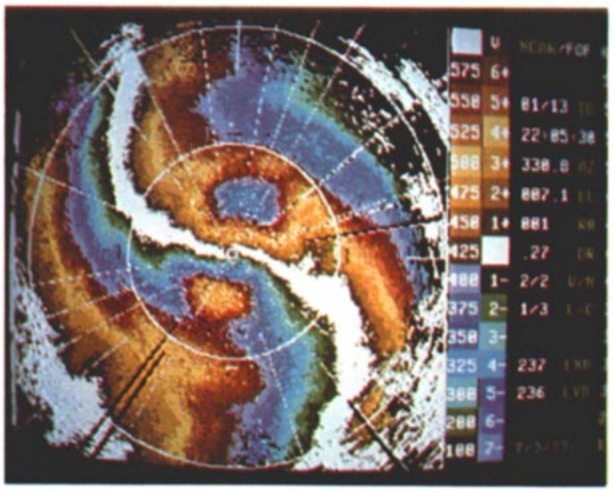

Fig. 3. Color display typical of warm air advection. Picture is for 2205 PST 13 January 1976, Tacoma, elevation 7.1°. Range marks at 20 and 40 km, north at top of picture, velocity color code in the right column. The zero-velocity band bisecting the picture in the shape of an S indicates winds veering from south near the ground to west-southwest aloft. Continuing color changes to the west-southwest and east-northeast out to full range also indicate that the veering winds extend to the echo top.

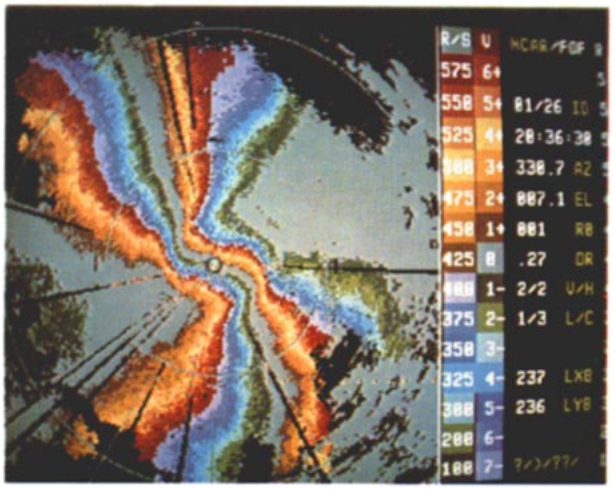

Fig. 4. Color display typical of a warm front. Picture is for 2036 PST 26 January 1976, Tacoma, elevation 7.1°, range marks at 20 and 40 km. Confinement of the S-shape of the zero-velocity band to the lowest 1.2 km (to 10 km slant range), and the two pie-shaped grey wedges extending in from 40 to 10 km slant range, indicate that the veering wind is confined to the lowest 1.2 km and place the warm frontal surface at 1.2 km.

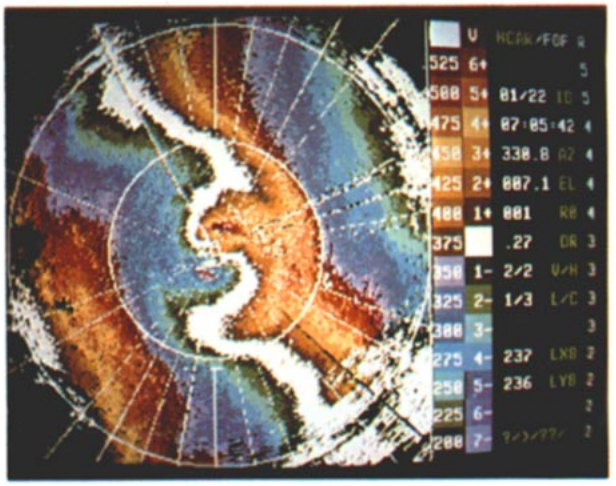

Fig. 5. Color display indicating an occlusion with warm air advection near the surface and cold air advection aloft. Picture is for 0705 PST 22 January 1976, Tacoma, elevation 7.1°, range marks at 20 and 40 km. The S within 15 km slant range indicates veering winds and warm air advection to a height of 1.9 km. Beyond 15 km the zero-velocity band traces a counterclockwise spiral, indicating backing winds and cold air advection.

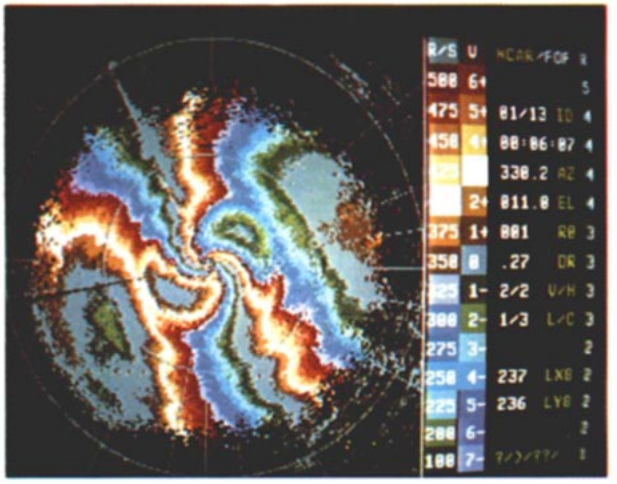

Fig. 7. Color display of two velocity maxima at 0006 PST 14 January 1976 (date incorrect in picture). Elevation 11° range marks at 20 and 40 km. Each velocity maximum produces a pair of oval-shaped rings, one upwind and one downwind. The lower velocity maximum core is horizontal, appearing at the same slant range (10 km) both upwind and downwind. The upper velocity maximum core slopes upward, appearing at a greater slant range downwind than upwind.

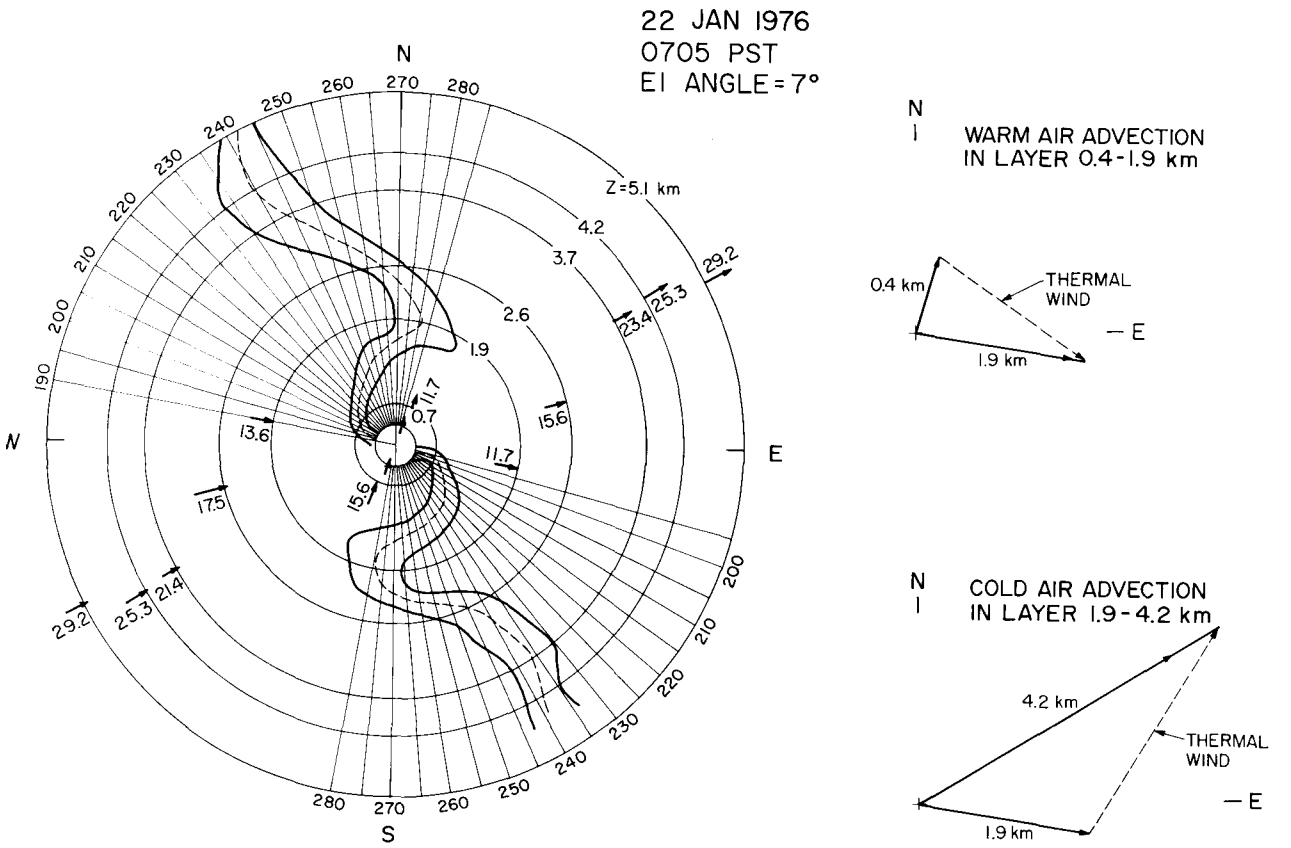

FIG. 6. Elements derived from the color display shown in Fig. 5. Wind directions are obtained from the zero-velocity band bisecting the figure by subtracting 90° from the azimuth on the low-pressure northwest side or adding 90° to the azimuth on the high-pressure southeast side. The two direction scales make this adjustment. Upwind and downwind speeds read from the color display are shown on the height contours. The hodographs confirm warm-air advection in the layer of veering winds and cold-air advection in the layer of backing winds.

Occasionally convergence may be suspected by inspection of the color display. Fig. 3 is an example. At a slant range of 20 km ($z=2.5$ km) the maximum radial speed downwind (northeast sector) nearly coincides with the "folded over" contour (red to purple) of 14.60 m s^{-1}, whereas upwind of the radar (southwest sector) the display shows three colors, or nearly 6 m s^{-1} greater than the "folded over" contour. The discussion in section 5 verifies the presence of convergence, at the same height, 30 min later than the time of Fig. 3.

4. Comparison with rawinsonde data

Wind profiles were obtained from the radar color display using the procedure described in the caption of Fig. 6. Three comparisons between radar wind profiles and simultaneous rawinsonde data, obtained at the University of Washington in Seattle, 45 km north of the radar site, are illustrated in Fig. 8. Since the observations were taken during periods of frontal passages, some differences in the soundings are to be expected due to atmospheric spatial variations. In spite of this, the results from the two independent methods are very similar.

During CYCLES the antenna scan sequence included a series of conical scans, vertically pointing observations and RHI scans. A single 360° conical scan, with elevation fixed, required 36 s and the sequence of 4°, 7°, 11°, 15° and 19° conical scans was repeated as often as every 7 min. These data provided a valuable supplement to the conventional rawinsondes which were obtained no more frequently than every 45 min.

5. Divergence computations

Procedures of computing divergence from Doppler radar data are described by Caton (1963) and by Browning and Wexler (1968). While their techniques were applied to digitally recorded data, the underlying principles are readily adapted to photographs of the color display.

Divergence may be evaluated from the expression

$$\mathrm{Div}=\frac{2}{R}\left[\frac{\bar{V}}{\cos\alpha}-\bar{V}_z\tan\alpha\right], \tag{3}$$

where $\bar{V}$ is the average radial velocity at an elevation angle α and a slant range of R during a 360° scan, and

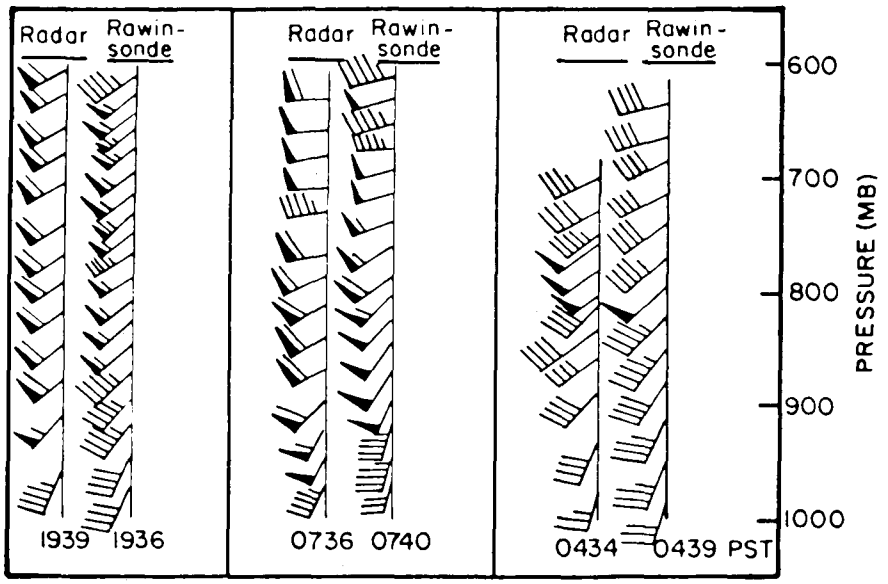

FIG. 8. Comparison of radar and rawinsonde wind data for 10 January 1976. Half wind barb is for 2.5 m s^{-1}, full barb is for 5 m s^{-1} and flag is for 25 m s^{-1}.

$\bar{V}_z$ is the mean vertical velocity of the precipitation particles. R is expressed in meters and velocities are in meters per second, positive away from the radar.

Generally, one is interested in a vertical profile of divergence, and in order that the profile may apply over the same horizontal area one must use a series of scans at different elevation angles. Our procedure is to compute $\bar{V}$ at a slant range of 20 km, the inner range marker on the color display, at elevation angles of 4°, 7°, 11°, 15° and 19° corresponding to heights of 1.55, 2.59, 3.97, 5.33 and 6.66 km above mean sea level. This series of scans is completed in about 7 min. The choice of 20 km complies with Browning and Wexler's recommendation that the slant range should be less than 23 km in order to reduce height errors.

Color transparencies for each elevation angle are projected onto polar coordinate graph paper. The 20 km range mark and the location of all color transitions at 20 km are traced in pencil onto the graph paper. This produces a diagram similar to the inner portion of Fig. 2. Then, proceeding in 6° steps around the 20 km circle, radial velocities are determined for each step and $\bar{V}$ is computed from

$$\bar{V} = \sum_{i=1}^{60} \bar{v}_i/60, \qquad (4)$$

where $\bar{v}_i$ is the mean radial velocity of the color band intercepted at the ith step.

Vertical velocities of precipitation particles [$\bar{V}_z$ in Eq. (3)] can be estimated by pointing the antenna vertically. During the CYCLES Project vertically pointing scans are interspersed regularly with the conical scans. Generally small fallspeeds, characteristic of snow, were observed as one would expect with the low freezing levels. Fallspeed spectra were recorded during the CYCLES Project and these spectra have been used to remove the influence of ground clutter in estimating average vertical velocities of the precipitation particles.[3] During 23 min of vertical scanning, between 2208 and 2258 PST on 13 January 1976, the vertical velocities given in Table 1 were observed. These values of $\bar{V}_z$ are believed to be representative of Pacific Northwest storms and were used to obtain the divergence profile given in Table 1. The magnitudes of the convergence and divergence in this case are consistent with the results of Matsumoto *et al.* (1967) who found, from measurements with closely spaced rawinsondes, that divergence in the mesoscale precipitation areas of winter storms over Japan was $\sim 10^{-4}$ s^{-1}.

Errors in the estimates of divergence that are peculiar to this procedure can be evaluated. Since only the term

TABLE 1. Mean vertical velocity $\bar{V}_z$ of precipitation particles, ground clutter effects removed, positive upward, between 2208 and 2258 PST, and divergence at 2237 PST 13 January 1976.

Height (km MSL)	1.55	2.59	3.97	5.33	6.66
$\bar{V}_z$ (m s^{-1})	−1.9	−1.2	−1.0	−0.8	−0.7
Divergence (10^{-4} s^{-1})	−1.62	−1.07	−0.44	+1.05	+1.37

[3] When vertically pointing, a second data system was activated which digitized the raw Doppler signals and recorded them on digital magnetic tape. Doppler spectra were computed later from the complex time series using a fast-Fourier transform algorithm and general purpose computer. Bias of the mean velocity estimates due to ground clutter was eliminated by removing the zero velocity spectral line from the spectrum. The mean vertical Doppler velocities were then obtained from the spectra using the objective thresholding method of Hildebrand and Sekhon (1974) to remove bias effects due to the background noise spectral density.

$2\bar{V}/R\cos\alpha$ in Eq. (3) is derived by this procedure, we can obtain the desired error estimates by determining $\sigma_{\bar{v}}$, the standard deviation of $\bar{V}$, and evaluating $(2/R\cos\alpha)\sigma_{\bar{v}}$.

From the expression for $\bar{V}$ in Eq. (4) we have for the variance of $\bar{V}$

$$\mathrm{Var}(\bar{V}) = \sum_{i=1}^{60} (1/60)^2 \,\mathrm{Var}(\bar{v}_i), \tag{5}$$

and since $\bar{v}_i$ is obtained by rounding off within an interval of approximately 2 m s^{-1}

$$\mathrm{Var}(\bar{v}_i) = 2^2/12 = \tfrac{1}{3}\ \mathrm{m^2\ s^{-2}}.$$

Thus from Eq. (5) we obtain $\sigma_{\bar{v}} = 0.07$ m s^{-1} and the divergence errors peculiar to this procedure are found to be 0.07×10^{-4} s^{-1} at a height of 1.55 km, increasing to 0.08×10^{-4} s^{-1} at 6.66 km. Since these errors are an order of magnitude smaller than the divergence estimates of Table 1, the procedure is evidently quite accurate.

6. Conclusions

Experience using the NCAR CP-3 radar in the University of Washington's CYCLES Project has shown that colored Doppler velocity patterns provide a variety of useful information in real time on the wind field in situations of widespread precipitation. These displays do not substitute for the more precise and accurate motion field analyses that may be performed after the fact. Rather, they augment such analyses by permitting meteorologists to identify significant features that are likely candidates for further analysis. The displays permit rapid measurements of wind speed and direction as a function of height, and divergence which can be computed from pictures of the radar color display with suitable speed and accuracy for mesoscale analysis. Readily recognizable patterns in the color displays have shown warm and cold advection layers, wind maxima and zones of difluence or confluence. Warm advection is indicated by an S-shaped zero velocity band, while cold advection is indicated by a backward S. Maximum wind layers appear as concentric color rings around a maximum velocity core. Difluence or confluence is indicated by asymmetry in the zero-velocity band. The displays also permit the meteorologist to optimize his data collection methodology through real-time decision making, thus concentrating his instrument resources (radars, aircraft, rawinsonde, etc.) on the most interesting situations.

Acknowledgments. The CYCLES Project is supported by Grant ATM 74-14726-A02 to the University of Washington from the Meteorology Program of the Atmospheric Research Section of the National Science Foundation. The successful operation of the radar was due to the skill and dedication of NCAR technicians Robert Bowie, Alan Sorenson and Dale Zalewski. Thomas J. Matejka of the University of Washington assisted in the collection of data.

REFERENCES

Battan, L. J., 1973: *Radar Observation of the Atmosphere.* The University of Chicago Press, 324 pp.

Browning, K. A., and R. Wexler, 1968: The determination of kinematic properties of a wind field using Doppler radar. *J. Appl. Meteor.*, **7**, 105–113.

——, M. E. Hardman, T. W. Harrold and C. W. Pardoe, 1973: The structure of rainbands within a mid-latitude depression. *Quart. J. Roy. Meteor. Soc.*, **99**, 215–231.

Caton, P. A. F., 1963: Wind measurement by Doppler radar. *Meteor. Mag.*, **92**, 213–222.

Elliott, R. D., and E. L. Hovind, 1965: Heat, water, and vorticity balance in frontal zones. *J. Appl. Meteor.*, 4, 196–211.

Gray, G. R., R. J. Serafin, D. Atlas, R. E. Rinehart and J. J. Boyajian: 1975: Real-time color Doppler radar display. *Bull. Amer. Meteor. Soc.*, **56**, 580–588.

Hildebrand, Peter H., and R. S. Sekhon, 1974: Objective determination of the noise level in Doppler spectra. *J. Appl. Meteor.*, **13**, 808–811.

Houze, R. A., Jr., J. D. Locatelli and P. V. Hobbs, 1976: Dynamics and cloud microphysics of the rainbands in an occluded front. *J. Atmos. Sci.*, **33**, 1921–1936.

Kreitzberg, Carl W., 1964: The structure of occlusions as determined from serial ascents and vertically-directed radar. Res. Rep. AFCRL-64-26, Air Force Cambridge Research Laboratories, 121 pp.

——, and H. A. Brown, 1970: Mesoscale weather systems within an occlusion. *J. Appl. Meteor.*, **9**, 417–432.

Lhermitte, R. H., 1972: Real time processing of meteorological Doppler radar signals. *Preprints 15th Radar Meteorology Conf.*, Champaign-Urbana, Amer. Meteor., Soc. 364–367.

——, and D. Atlas, 1961: Precipitation motion by pulse Doppler. *Preprints Ninth Radar Meteorology Conf.*, Kansas City, Amer. Meteor. Soc., 218–223.

Matsumoto, S., K. Nimomiya and T. Akiyama, 1967: Cumulus activities in relation to the mesoscale convergence field. *J. Meteor. Soc. Japan*, **45**, 292–304.